Application of SCU technology for hard X-rays production at the European XFEL

Dr Barbara Marchetti
UNSYS department – EuXFEL GmbH
Undulator Scientist

UK Accelerator Institutes Seminar Series
27.04.23

Credits

Superconducting undulator activities for European XFEL

European XFEL GmbH

S. Casalbuoni (group leader UNSYS), S. Abeghyan, L. Alankyan, J. Baader, M. B. Shanjani, U. Englisch, V. Grattoni, S. Karabekyan, F. Preisskorn, G. Yakopov, M. Yakopov, P. Ziolkowski

H. Sinn

D. La Civita, M. Di Felice

G. Geloni, C. Lechner

DESY

W. Decking, R. Wichmann

S. Liu, E. Shneydmiller, I. Zagorodnov

S. Barbanotti, K. Jensch, T. Schnautz

H.-J. Eckoldt, A. Hauberg, C. Helwich, R. Zimmermann

S. Lederer, L. Lilje, T. Wohlenberg

Bilfinger Noell GmbH

W. Walter
A. Hobl
A. Vagatin

A. Potter (*University of Liverpool*)

A. Grau (*KIT*)

Outline

- Introduction to X-rays, X-rays production using charged particles
- X-ray FEL facilities and peculiarities of European XFEL
- SCU technology: motivation for development program on superconducting undulators
- SCU afterburner for SASE2: S-PRESSO and FESTA at European XFEL
- Characterization of SCU coils: SUNDAE1 and SUNDAE2 test-stands
- Summary and conclusions

X-rays

- Discovered in **1895** by Wihlhelm Konrad **Röntegen**
- Penetrate materials optically **opaque in the visible range**, different absorption by materials of different **density**, **composition** and **homogeneity**
- Wavelengths of **atomic dimension**
- **Ionizing** radiation

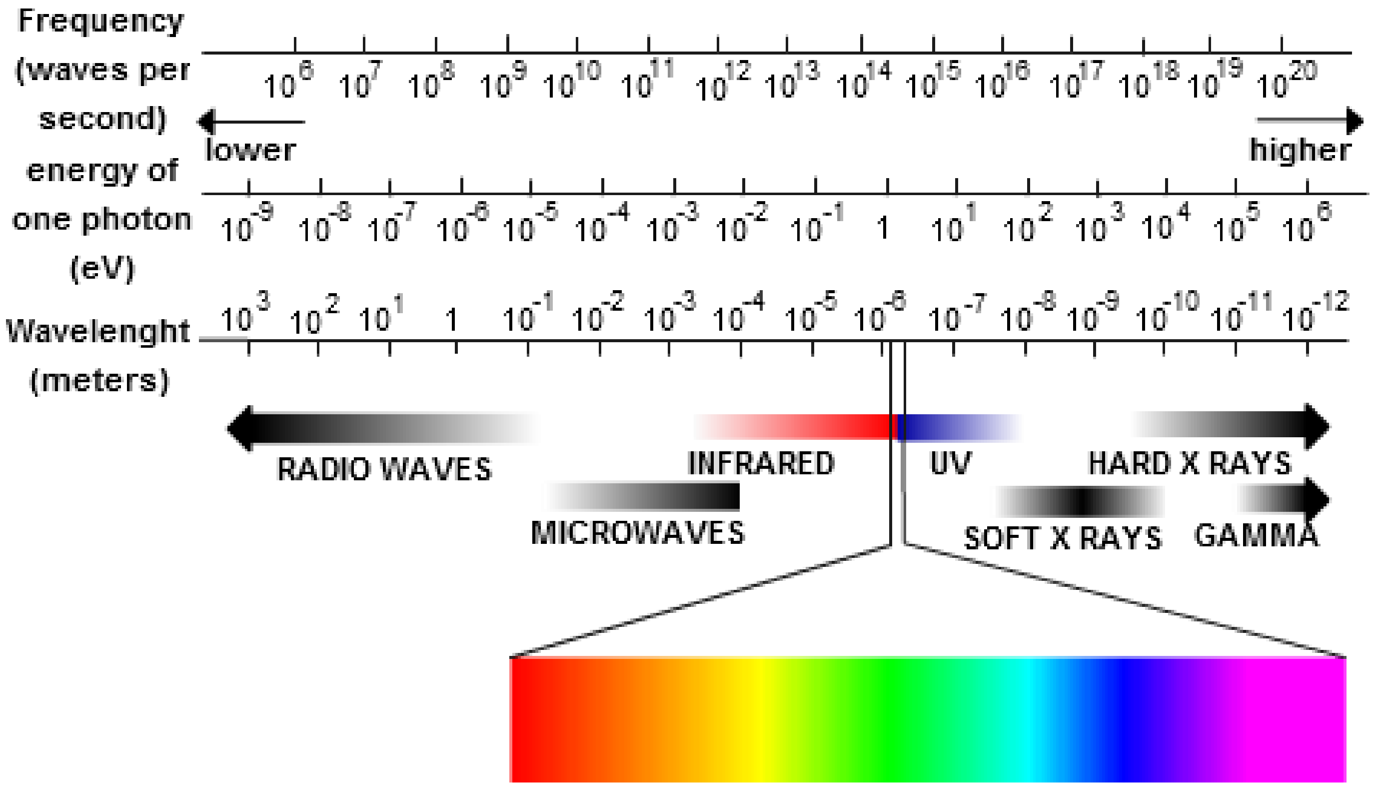

Credits: https://www.nde-ed.org/Physics/X-Ray/nature.xhtml

Applications of X-rays

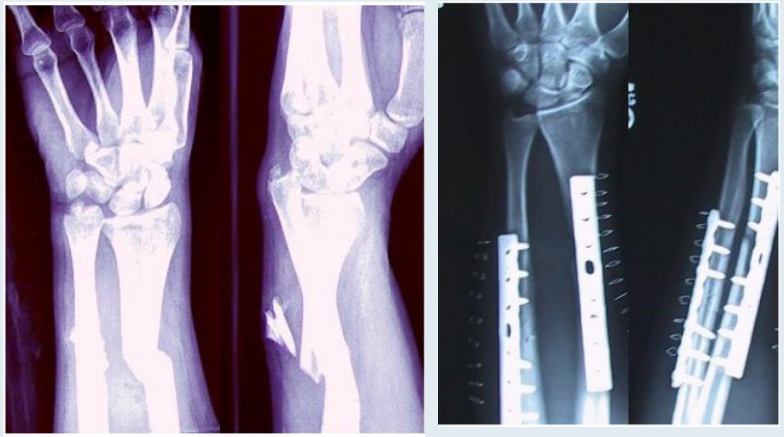

Figure credits:
https://en.wikipedia.org/wiki/Bone_fracture#mediaviewer/File:Broken_fixed_arm.jpg

Medicine:

- Imaging
- Radiation therapy

Industry:

- Security checks
- Diagnostics of cracks or flaws in materials
- Diagnostics to analyze the structure of materials

Figure credits:
https://coruzant.com/health-tech/industrial-applications-of-x-ray-radiation/

Science:

- Crystallography
- Spectroscopy

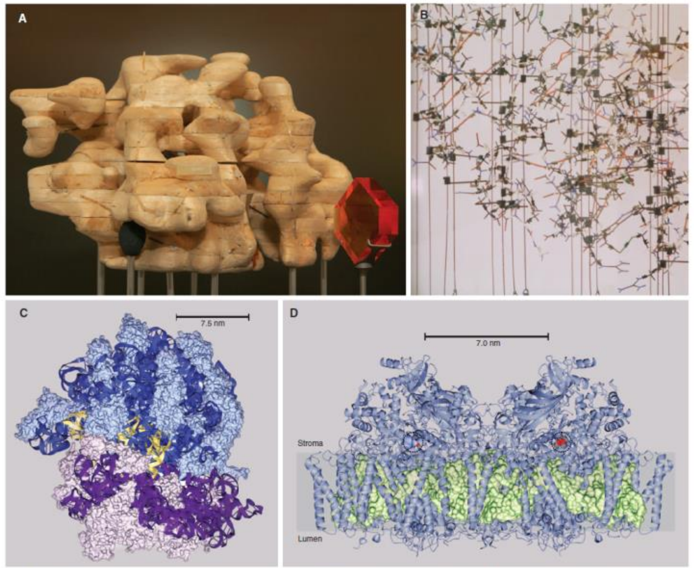

Fig. 1. Visualization of macromolecular structures. (**A**) Balsa wood model of myoglobin at 5 Å resolution (*45*) and a model of a monoclinic crystal, made by H. Scouloudi, 1969. (**B**) Wire model of lysozyme structure (*39*). Model constructed by W. Browne and M. Pickford circa 1965. Refurbished by A. Todd and Unicol Engineering of Headington, Oxford, UK. Blue, nitrogen; red, oxygen; black, carbon; yellow, sulfur; and gray, hydrogen bonds. (**C**) Ribosome 70*S* particle at 3.5 Å resolution (*46*). 30*S* subunit and tRNA, PDB entry 2wdk; 50*S* subunit, PDB entry 2wdl. The 30*S* subunit is shown in purple (pale for protein, dark for RNA) and the 50*S* subunit in blue (pale for protein, dark for RNA). The tRNA is in gold. Figure made with CCP4mg (*47*). (**D**) Photosystem II at 1.9 Å resolution. PDB entry 3arc (*48*). The protein is shown in blue and the chlorophylls in green. The oxygen-evolving cluster is depicted as spheres and highlighted by dotted circles, and the membrane bilayer is indicated by a shaded box. Figure made with CCP4mg.

REVIEW

Developments in X-ray Crystallographic Structure Determination of Biological Macromolecules

Elspeth F. Garman

7 MARCH 2014 VOL 343 **SCIENCE** www.sciencemag.org

Methods to produce X-rays from the acceleration of charged particles

Methods to produce X-rays from the acceleration of charged particles

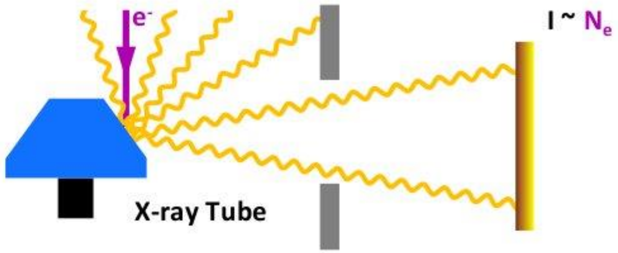

- a beam of high-energy electrons impinges on a solid target
- Bremsstrahlung ("braking radiation") + characteristic peaks atomic transition
- photons emitted in all directions

Figure credits:
A. Shabalin, „Coherent X-ray diffraction studies of mesoscopic materials"
DOI: 10.13140/RG.2.1.4004.5680

Methods to produce X-rays from the acceleration of charged particles

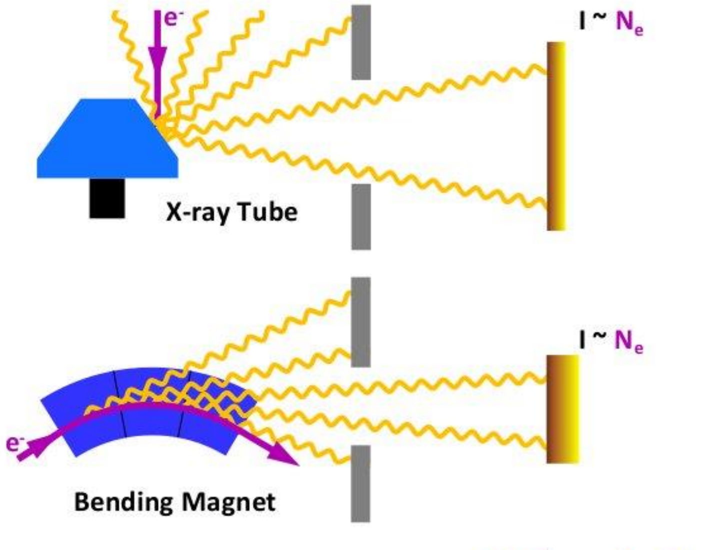

- a beam of high-energy electrons impinges on a solid target
- Bremsstrahlung (“braking radiation”) + characteristic peaks atomic transition
- photons emitted in all directions

- the charged particles are deflected by the magnetic fields
- synchrotron radiation (spectrum from THz to hard X-rays)
- radiation emission cone θ=1/γ

Figure credits:
A. Shabalin, „Coherent X-ray diffraction studies of mesoscopic materials“
DOI: 10.13140/RG.2.1.4004.5680

Methods to produce X-rays from the acceleration of charged particles

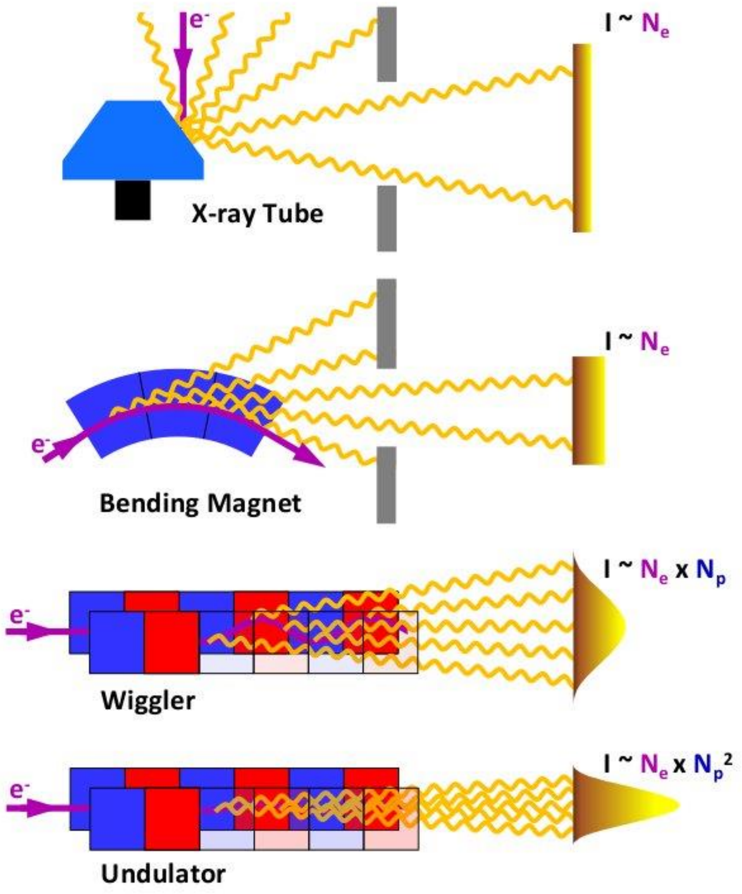

- a beam of high-energy electrons impinges on a solid target
- Bremsstrahlung (“braking radiation”) + characteristic peaks atomic transition
- photons emitted in all directions

- the charged particles are deflected by the magnetic fields
- synchrotron radiation (spectrum from THz to hard X-rays)
- radiation emission cone $\theta=1/\gamma$

- Angular excursion >> synchrotron radiation’s opening angle ($1/\gamma$)
- The radiation cones from each magnet do not overlap

- Angular excursion =< synchrotron radiation’s opening angle ($1/\gamma$)
- The radiation cones from each magnet overlap → constructive interference for some wavelengths → discrete spectrum

Figure credits:
A. Shabalin, „Coherent X-ray diffraction studies of mesoscopic materials“
DOI: 10.13140/RG.2.1.4004.5680

Methods to produce X-rays from the acceleration of charged particles

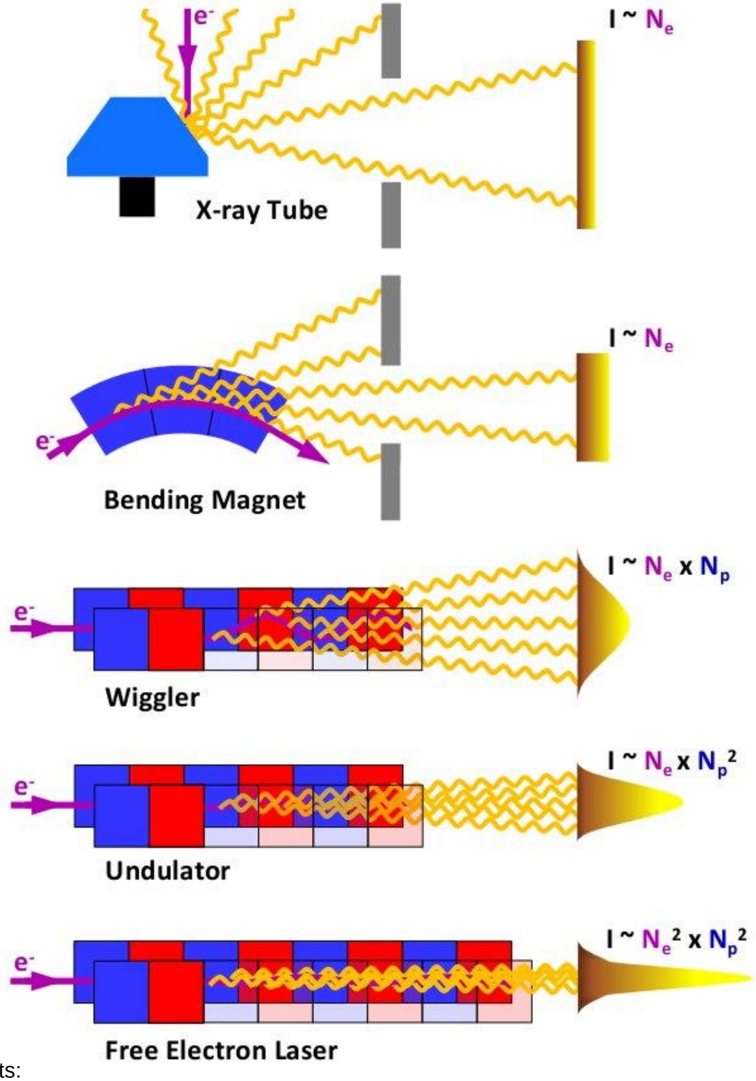

- a beam of high-energy electrons impinges on a solid target
- Bremsstrahlung (“braking radiation”) + characteristic peaks atomic transition
- photons emitted in all directions

- the charged particles are deflected by the magnetic fields
- synchrotron radiation (spectrum from THz to hard X-rays)
- radiation emission cone θ=1/γ

- Angular excursion >> synchrotron radiation’s opening angle (1/γ)
- The radiation cones from each magnet do not overlap

- Angular excursion =< synchrotron radiation’s opening angle (1/ γ)
- The radiation cones from each magnet overlap → constructive interference for some wavelengths → discrete spectrum

- Constructive interference + e-beam microbunching
- Discrete spectrum and exponential amplification

Figure credits:
DOI: 10.13140/RG.2.1.4004.5680

Main differences between synchrotrons and FELs

Table 1.1 Comparison of orders of magnitude synchrotron and XFEL radiation† properties. †XFEL values derive from LCLS unless otherwise stated. 8-keV photons assumed. *EuroXFEL time structure: 2700 pulses at 4.5 MHz, 10 such bursts per second. **photons s^{-1} 0.1% BW^{-1}. ‡After Si(111) monochromator, $\Delta\nu/\nu = 1.4 \times 10^{-4}$. ¶Unmonochromatized, full SASE spectrum. §23 kW during pulse burst

Property	Synchrotron	XFEL
$\Delta\tau$	50 – 400 ps	1 – 100 fs
Δt	5 ns	$10^{-2} - 2 \times 10^{-7}$ s*
Average flux**	2×10^{14}	10^{14}
Peak flux**	6×10^{15}	2×10^{25}
$\#h\nu$/pulse	4×10^{4} ‡	4×10^{12} ¶
Peak power	1 W ‡	10^{11} W¶
Average power	25 mW‡	600 mW¶ – 140 W¶*§

XFELs opened the possibility to study matter at **atomic-level spacial scales** and **femtosecond time scales** for the first time

Reference:
Willmott, P.R. (2021). X-Ray Sources at Large-Scale Facilities. In: Bulou, H., Joly, L., Mariot, JM., Scheurer, F. (eds) Magnetism and Accelerator-Based Light Sources. Springer Proceedings in Physics, vol 262. Springer, Cham. https://doi.org/10.1007/978-3-030-64623-3_1

XFEL Facilities

Table 1. Major parameters for worldwide X-ray FEL facilities

Facility	Beam energy (GeV)	Photon energy (eV)	Repetition rate (Hz)	Pulse duration (FWHM) (fs)
FLASH	0.35–1.25	14–620	4×10^3 to 10^6	10–200
LCLS	2.5–16.9	280–12,800	120	5–400
SACLA	5.1–8.5	4,000–20,000	60	2–10
FERMI	1–1.5	20–310	50	30–100
PAL-XFEL	3.5–10	275–20,000	60	5–100
SwissFEL	2.1–5.8	250–1,240	100	1–20
European XFEL	8.5–17.5	240–25,000	2.7×10^4	3–150
SXFEL	1.0–1.6	124–1,000	50	30–1,000
LCLS-II (HE)	4–15	200–25,000	$120/10^6$	1–500
SHINE	8	400–25,000	10^6	3–600

Note that only a portion of their performance is listed here for indication. In addition, the pulse duration varies with the operating mode of the facility, such as low charge and two-color mode. More detailed information can be found on their websites.

Features and futures of X-ray free-electron lasers

Nanshun Huang,[1,2] Haixiao Deng,[1,3,*] Bo Liu,[1,3] Dong Wang,[1,3] and Zhentang Zhao[1,3,*]
*Correspondence: denghaixiao@zjlab.org.cn (H.D.); zhaozhentang@zjlab.org.cn (Z.Z.)
Received: November 12, 2020; Accepted: March 14, 2021; Published Online: March 17, 2021; https://doi.org/10.1016/j.xinn.2021.100097

XFEL Facilities

Table 1. Major parameters for worldwide X-ray FEL facilities

Facility	Beam energy (GeV)	Photon energy (eV)	Repetition rate (Hz)	Pulse duration (FWHM) (fs)
FLASH	0.35–1.25	14–620	4×10^3 to 10^6	10–200
LCLS	2.5–16.9	280–12,800	120	5–400
SACLA	5.1–8.5	4,000–20,000	60	2–10
FERMI	1–1.5	20–310	50	30–100
PAL-XFEL	3.5–10	275–20,000	60	5–100
SwissFEL	2.1–5.8	250–1,240	100	1–20
European XFEL	8.5–17.5	240–25,000	2.7×10^4	3–150
SXFEL	1.0–1.6	124–1,000	50	30–1,000
LCLS-II (HE)	4–15	200–25,000	$120/10^6$	1–500
SHINE	8	400–25,000	10^6	3–600

Note that only a portion of their performance is listed here for indication. In addition, the pulse duration varies with the operating mode of the facility, such as low charge and two-color mode. More detailed information can be found on their websites.

- First **MHz hard X-ray** free electron laser
- **Highest** e-beam **energy**

Features and futures of X-ray free-electron lasers

Nanshun Huang,[1,2] Haixiao Deng,[1,3,*] Bo Liu,[1,3] Dong Wang,[1,3] and Zhentang Zhao[1,3,*]
*Correspondence: denghaixiao@zjlab.org.cn (H.D.); zhaozhentang@zjlab.org.cn (Z.Z.)
Received: November 12, 2020; Accepted: March 14, 2021; Published Online: March 17, 2021; https://doi.org/10.1016/j.xinn.2021.100097

nature photonics ARTICLES
https://doi.org/10.1038/s41566-020-0607-z
Check for updates

A MHz-repetition-rate hard X-ray free-electron laser driven by a superconducting linear accelerator

Undulator lines at European XFEL

Planar permanent magnet undulators

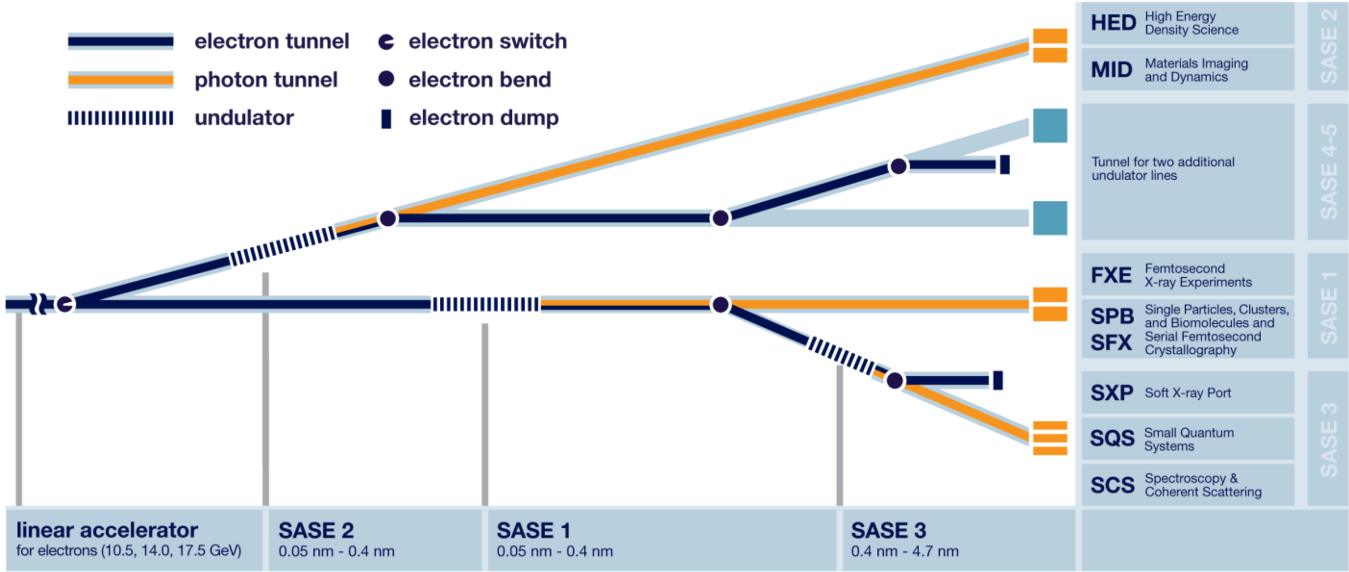

- Undulator parameter:

$$K = \frac{e}{2\pi mc} B_0 \lambda_U$$

SASE1/2 hard X-rays beamlines:

- Radiation range:
  - γ energy: 3-25 keV
  - γ wavelength: 4 Å – 0.5 Å
- **Planar undulators:**
  - Period length: 40 mm
  - K range: 1.65-3.9

SASE3 soft X-rays beamline:

- Radiation range:
  - γ energy: 0.26-3 keV
  - γ wavelength: 4.7 nm – 4 Å
- **Planar undulators:**
  - Period length: 68 mm
  - K range: 4-9
- **Helical afterburner:**
  - Period length: 90 mm
  - K range (C+, C-, LH, LV): 3.37-9.4

Why superconducting undulators?

Wider tunability of the **photon beam wavelength λ_R** while keeping the electron beam energy constant

Why superconducting undulators?

Wider tunability of the **photon beam wavelength λ_R** while keeping the electron beam energy constant

Reduction of the undulator period: shorter λ_R possible

$$K = \frac{e}{2\pi mc} B_0 \lambda_U = 0.9336\, B_0[T] \lambda_U[cm]$$

$$\lambda_R = \frac{\lambda_U}{2n\gamma^2}\left(1 + \frac{K^2}{2} + \gamma^2\theta^2\right)$$

$\lambda_U \downarrow$
$\lambda_R \downarrow$

Enables achieving harder X-rays

Why superconducting undulators?

Wider tunability of the **photon beam wavelength λ_R** while keeping the electron beam energy constant

Reduction of the undulator period: shorter λ_R possible

$$K = \frac{e}{2\pi mc} B_0 \lambda_U = 0.9336\, B_0[T] \lambda_U[cm]$$

$$\lambda_R = \frac{\lambda_U}{2n\gamma^2}\left(1 + \frac{K^2}{2} + \gamma^2\theta^2\right)$$

$\lambda_U \downarrow$
$\lambda_R \downarrow$

Enables achieving harder X-rays

Increase of the peak field on axis B: Re-establish tunability of λ_R towards longer wavelengths

$$\lambda_R = \frac{\lambda_U}{2n\gamma^2}\left(1 + \frac{K^2}{2} + \gamma^2\theta^2\right)$$

$$K = \frac{e}{2\pi mc} B_0 \lambda_U = 0.9336\, B_0[T] \lambda_U[cm]$$

$B_0 \uparrow$ Online
$\lambda_R \uparrow$ tunable

Guarantees wide range of tunability

Why superconducting undulators?

Wider tunability of the **photon beam wavelength λ_R** while keeping the electron beam energy constant

- Shifts the tuning-mechanism **from the electron beam side** (electron energy) **to the undulators side** (magnetic field)
- Potentially simplifies FEL adjustment for user requirements on different beamlines

→

- Cost reduction on the accelerator (smaller E-beam energy needed)

Why superconducting undulators?

Wider tunability of the **photon beam wavelength λ_R** while keeping the electron beam energy constant

- Shifts the tuning-mechanism **from the electron beam side** (electron energy) **to the undulators side** (magnetic field)
  - Potentially simplifies FEL adjustment for user requirements on different beamlines

→ Cost reduction on the accelerator (smaller E-beam energy needed)

SC technology allows producing undulators with very short period length

→ Undulators with shorter periods but same K have shorter saturation length → more compact FELs (reduction of civil construction costs)

Why superconducting undulators?

Wider tunability of the **photon beam wavelength λ_R** while keeping the electron beam energy constant

- Shifts the tuning-mechanism **from the electron beam side** (electron energy) **to the undulators side** (magnetic field)
- Potentially simplifies FEL adjustment for user requirements on different beamlines

→ Cost reduction on the accelerator (smaller E-beam energy needed)

SC technology allows producing undulators with very short period length

→ Undulators with shorter periods but same K have shorter saturation length → more compact FELs (reduction of civil construction costs)

Better **radiation hardness** than PM (demonstrated in NbTi magnets used in colliders - Tevatron, HERA, LHC)

All values are scaled to gap value of 5mm

Developments to increase B_{max} in undulators

Permanent magnet undulator

IVU = in-vacuum undulator

CPMU = cryogenic permanent magnet undulator

SCU = superconducting undulator

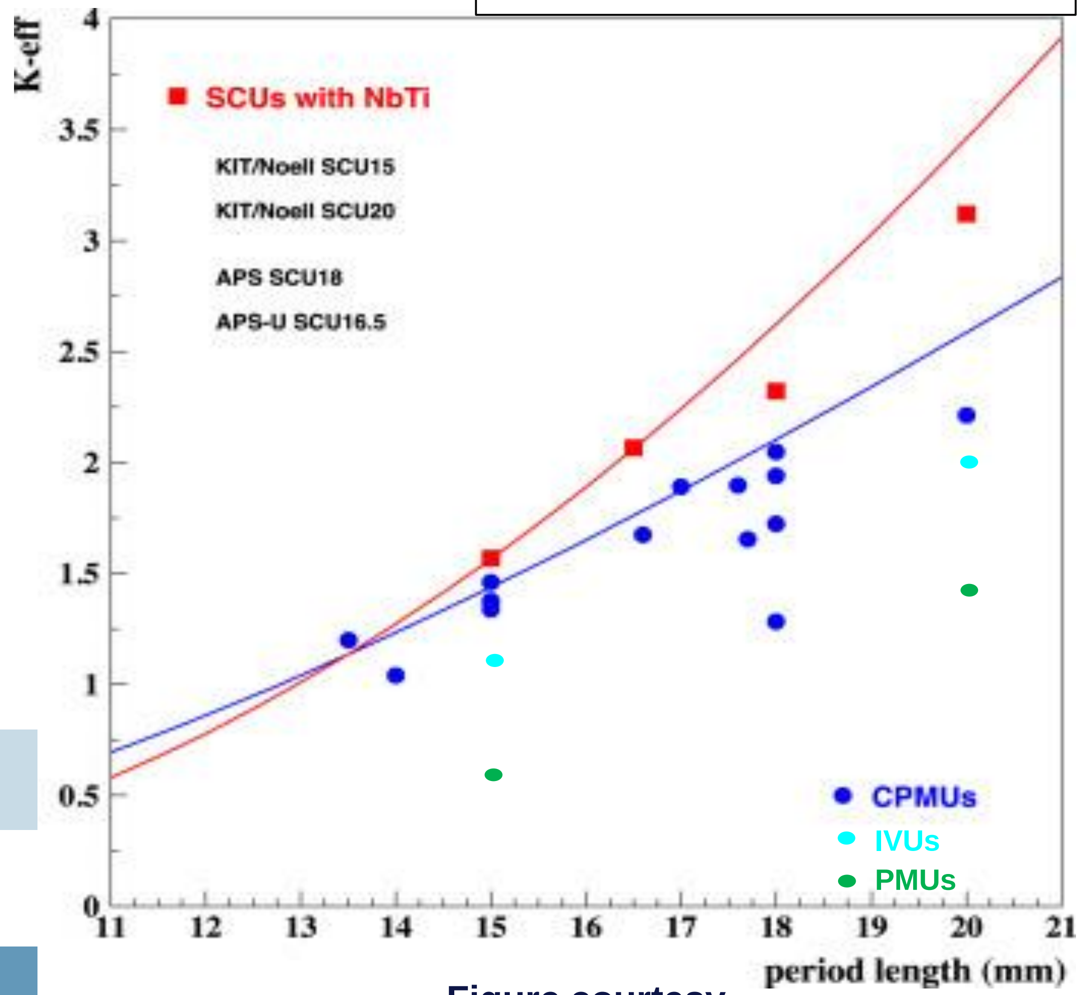

Figure courtesy
J. Bahrdt, E. Gluskin, NIMA (2018)
+
S. Casalbuoni
“Superconductive undulator development” (talk 2020)
scaling values from
P. Elleaume et. al NIM A 455 (2000) 503-523

The cooling at colder temperature would be beneficial : scaling of K versus temperature:

The peak field on axis increased by about 50 % with respect to NbTi at 4K

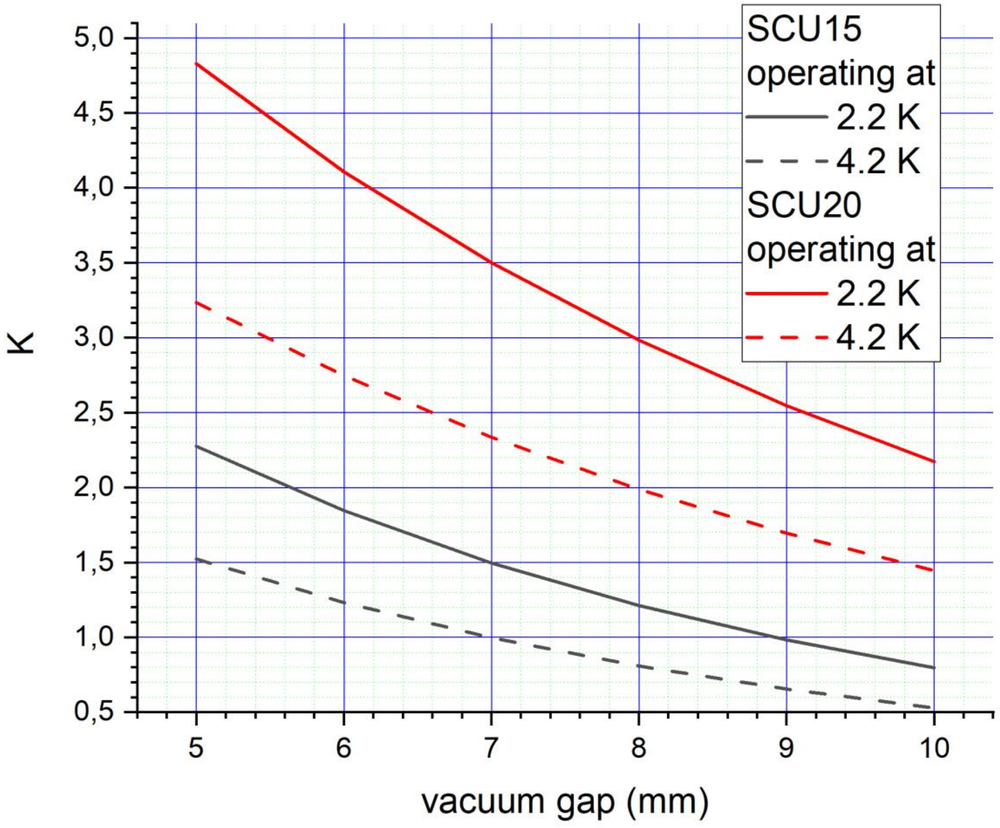

Calculation by Sara Casalbuoni

SCU technology (1/2)

- SCUs in **Synchrotron sources**

K. Zhang and M. Calvi, 2022 Supercond. Sci. Technol. 35 093001

Table 1. Summary of state-of-the-art developed SCU models, prototypes and devices. Model: full SCU coil assembly (testing coils and half coil assemblies are not included). Prototype: full SCU coil assembly + vacuum chamber + cryostat. Device: full SCU coil assembly + vacuum chamber + cryostat + beam commissioned.

SCU type	Conductor	Year	Laboratory	No of periods	Period length (mm)	Magnetic bore/gap (mm)	Vacuum bore/gap (mm)	Peak on-axis field (T)	Type
Helical	NbTi wire	1973	Stanford U. [9]	160	32.3	9.8	8	$V(H) = 1.30$	Device
		1974	Stanford U. [9]	160	32.3	12.5	10.2	—	Device
		1992	BINP [15]	8	24	20	18	$V(H) = 0.47$	Device
		2002	Cornell U. [16]	64	2.4	1.5	0.9	$V(H) = 0.34$	Prototype
		2005	Kurchatov Inst. [11]	6	28	11	—	$V(H) = 1.06$	Model
		2005–07	STFC [19]	20	14	6	—	$V(H) = 0.9$	Model
		2005–07	STFC [19]	25	12	6	—	$V(H) = 0.53$	Model
		2005–07	STFC [19]	25	12	6	—	$V(H) = 0.96$	Model
		2005–07	STFC [19]	42	11.5	6.35	—	$V(H) = 0.82$	Model
		2008	STFC [19]	150	11.5	6.35	5.23	$V(H) = 1.13$	Prototype
		2018	ANL [12]	38.5	31.5	31	8	$V(H) = 0.41$	Device
	Nb_3Sn wire	2007	ANL [21]	17	14	7.94	—	$V(H) = 0.9$	Model
		2012	Ohio State U. [23]	17	14	8	—	$V(H) = 0.8$	Model
	MgB_2 wire	2009	Ohio State U. [24]	17	14	8	—	$V(H) = 0.25$	Model
Planar	NbTi wire	1980	PARIS XI [30]	23	40	22	12	$V = 0.45$	Device
		1990	BNL [51]	3	8.8	4.4	—	$V = 0.5$	Model
		1996	BNL [52]	23	8.8	4.4	3.8	$V = 0.51$	Prototype
		1998	KIT [32]	100	3.8	1	1	$V = 0.56$	Device
		2003	KIT/ACCEL [35]	10	14	5	—	$V = 1.33$	Model
		2006	KIT/ACCEL [36]	100	14	8	7.4	$V = 0.38$	Device
		2008	NSRRC [60]	20	15	5.6	—	$V = 1.45$	Model
		2011	NSRRC [61]	65	15	5.6	—	$V = 1.36$	Model
		2013	ANL [54]	20.5	16	9.5	7.2	$V = 0.8$	Device
		2015	KIT/Noell [28]	11.5	20	8	—	$V = 1.2$	Model
		2015	ANL [56]	59.5	18	9.5	7.2	$V = 0.98$	Device
		2016	SINAP [62]	5	16	8	—	$V = 0.93$	Model
		2016	KIT/Noell [26]	100.5	15	8	7	$V = 0.73$	Device
		2016	BINP [86]	15	15.6	8	—	$V = 1.2$	Model
		2018	BINP [87]	40	15.6	8	—	$V = 1.2$	Model
		2018	ANL [57]	70	21	8	—	$V = 1.67$	Model
		2019	KIT/Noell [42]	74.5	20	8	7	$V = 1.18$	Device
		2019	KIT [43]	24 or 12	17 or 34	6	—	$V = 1.3$ or 2.3	Model
		2019	STFC [48]	19	15.5	7.4	5.4	$V \geqslant 0.8$	Device
		2021	BINP [88]	119	15.6	8	—	$V = 1.2$	Model
		2021	SINAP [64]	50	16	10	7.5	$V = 0.62$	Device
		2021	IHEP [66]	30	15	7	—	$V = 1.01$	Model
	Nb_3Sn wire	2018	LBNL [48]	73	19	8	—	$V = 1.83$	Model
		2021	ANL [72]	28.5	18	9.5	—	$V = 1.2$	Model
	ReBCO tape	2014	LANL [80]	3	14	3.2	—	$V = 0.77$	Model
		2017	ANL [74]	5	16	9.5	—	$V = > 0.2$	Model
	ReBCO bulk	2013	Kyoto U. [104]	5	10	4	—	$V = 0.85$	Model
		2019	PSI [107]	5	10	6	—	$V = 0.85$	Model
		2021	PSI [3]	10	10	4	—	$V = 1.54$	Model
Variable	NbTi wire	2010	NSRRC [120]	4.5	24	6.8	—	$V(H) = 0.61$	Model
		2019	ANL [126]	15	30	—	6	$V(H) = 0.6$	Model
		2020	BINP [121]	14	22	8	—	$V = 1.0, H = 0.7$	Model

SCU technology (1/2)

- SCUs in **Synchrotron sources**
  - Karlsruhe Institute of Technology (KIT) in collaboration with company Babcock Noell GmbH (currently Bilfinger Noell GmbH)
    - ► Facility for beam heat load study and magnetic field characterization
    - ► Operation of 2 undulators at KIT light source

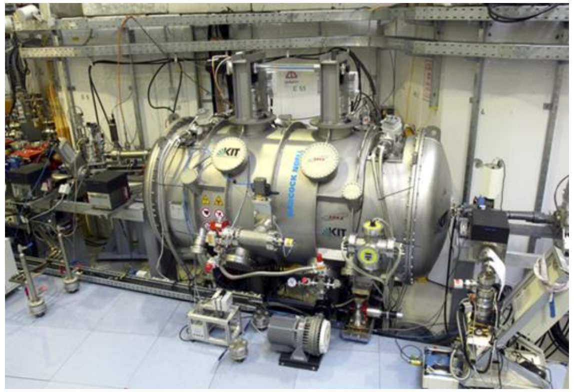

SCU15

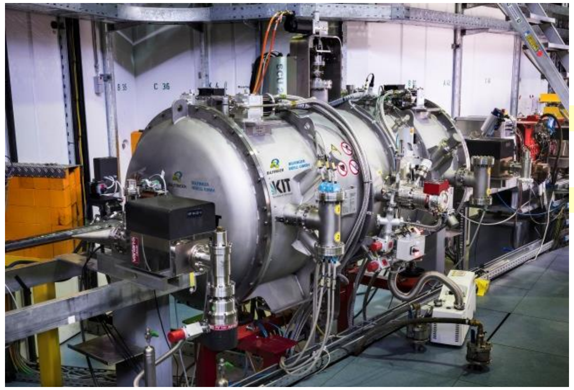

SCU20

S. Casalbuoni et al., Synchr. Rad. News, 31:3, 24-28 (2018)

K. Zhang and M. Calvi, 2022 Supercond. Sci. Technol. 35 093001

Table 1. Summary of state-of-the-art developed SCU models, prototypes and devices. Model: full SCU coil assembly (testing coils and half coil assemblies are not included). Prototype: full SCU coil assembly + vacuum chamber + cryostat. Device: full SCU coil assembly + vacuum chamber + cryostat + beam commissioned.

SCU type	Conductor	Year	Laboratory	No of periods	Period length (mm)	Magnetic bore/gap (mm)	Vacuum bore/gap (mm)	Peak on-axis field (T)	Type	
Helical	NbTi wire	1973	Stanford U. [9]	160	32.3	9.8	8	$V(H) = 1.30$	Device	
		1974	Stanford U. [9]	160	32.3	12.5	10.2	—	Device	
		1992	BINP [15]	8	24	20	18	$V(H) = 0.47$	Device	
		2002	Cornell U. [16]	64	2.4	1.5	0.9	$V(H) = 0.34$	Prototype	
		2005	Kurchatov Inst. [11]	6	28	11	—	$V(H) = 1.06$	Model	
		2005–07	STFC [19]	20	14	6	—	$V(H) = 0.9$	Model	
		2005–07	STFC [19]	25	12	6	—	$V(H) = 0.53$	Model	
		2005–07	STFC [19]	25	12	6	—	$V(H) = 0.96$	Model	
		2005–07	STFC [19]	42	11.5	6.35	—	$V(H) = 0.82$	Model	
		2008	STFC [19]	150	11.5	6.35	5.23	$V(H) = 1.13$	Prototype	
		2018	ANL [12]	38.5	31.5	31	8	$V(H) = 0.41$	Device	
	Nb_3Sn wire	2007	ANL [21]	17	14	7.94	—	$V(H) = 0.9$	Model	
		2012	Ohio State U. [23]	17	14	8	—	$V(H) = 0.8$	Model	
	MgB_2 wire	2009	Ohio State U. [24]	17	14	8	—	$V(H) = 0.25$	Model	
Planar	NbTi wire	1980	PARIS XI [30]	23	40	22	12	$V = 0.45$	Device	
		1990	BNL [51]	3	8.8	4.4	—	$V = 0.5$	Model	
		1996	BNL [52]	23	8.8	4.4	3.8	$V = 0.51$	Prototype	
		1998	KIT [32]	100	3.8	1	1	$V = 0.56$	Device	
		2003	KIT/ACCEL [35]	10	14	5	—	$V = 1.33$	Model	
		2006	KIT/ACCEL [36]	100	14	8	7.4	$V = 0.38$	Device	
		2008	NSRRC [60]	20	15	5.6	—	$V = 1.45$	Model	
		2011	NSRRC [61]	65	15	5.6	—	$V = 1.36$	Model	
		2013	ANL [54]	20.5	16	9.5	7.2	$V = 0.8$	Device	
		2015	KIT/Noell [28]	11.5	20	8	—	$V = 1.2$	Model	
		2015	ANL [56]	59.5	18	9.5	7.2	$V = 0.98$	Device	
		2016	SINAP [62]	5	16	8	—	$V = 0.93$	Model	
		2016	KIT/Noell [26]	100.5	15	8	7	$V = 0.73$	Device	ANKA
		2016	BINP [86]	15	15.6	8	—	$V = 1.2$	Model	
		2018	BINP [87]	40	15.6	8	—	$V = 1.2$	Model	
		2018	ANL [57]	70	21	8	—	$V = 1.67$	Model	
		2019	KIT/Noell [42]	74.5	20	8	7	$V = 1.18$	Device	ANKA
		2019	KIT [43]	24 or 12	17 or 34	6	—	$V = 1.3$ or 2.3	Model	
		2019	STFC [48]	19	15.5	7.4	5.4	$V \geqslant 0.8$	Device	
		2021	BINP [88]	119	15.6	8	—	$V = 1.2$	Model	
		2021	SINAP [64]	50	16	10	7.5	$V = 0.62$	Device	
		2021	IHEP [66]	30	15	7	—	$V = 1.01$	Model	
	Nb_3Sn wire	2018	LBNL [48]	73	19	8	—	$V = 1.83$	Model	
		2021	ANL [72]	28.5	18	9.5	—	$V = 1.2$	Model	
	ReBCO tape	2014	LANL [80]	3	14	3.2	—	$V = 0.77$	Model	
		2017	ANL [74]	5	16	9.5	—	$V = > 0.2$	Model	
	ReBCO bulk	2013	Kyoto U. [104]	5	10	4	—	$V = 0.85$	Model	
		2019	PSI [107]	5	10	6	—	$V = 0.85$	Model	
		2021	PSI [3]	10	10	4	—	$V = 1.54$	Model	
Variable	NbTi wire	2010	NSRRC [120]	4.5	24	6.8	—	$V(H) = 0.61$	Model	
		2019	ANL [126]	15	30	—	6	$V(H) = 0.6$	Model	
		2020	BINP [121]	14	22	8	—	$V = 1.0, H = 0.7$	Model	

SCU technology (1/2)

SCUs in **Synchrotron sources**

- Advanced Photon Source (APS) at ANL:
  - ► Specialized SCU facility
  - ► Operation of several SCU at the APS ring

Helical SCU installed in APS

M. Kasa et al. PRSTAB 23, 050701 (2020)

K. Zhang and M. Calvi, 2022 Supercond. Sci. Technol. 35 093001

Table 1. Summary of state-of-the-art developed SCU models, prototypes and devices. Model: full SCU coil assembly (testing coils and half coil assemblies are not included). Prototype: full SCU coil assembly + vacuum chamber + cryostat. Device: full SCU coil assembly + vacuum chamber + cryostat + beam commissioned.

SCU type	Conductor	Year	Laboratory	No of periods	Period length (mm)	Magnetic bore/gap (mm)	Vacuum bore/gap (mm)	Peak on-axis field (T)	Type	
Helical	NbTi wire	1973	Stanford U. [9]	160	32.3	9.8	8	$V(H) = 1.30$	Device	
		1974	Stanford U. [9]	160	32.3	12.5	10.2	—	Device	
		1992	BINP [15]	8	24	20	18	$V(H) = 0.47$	Device	
		2002	Cornell U. [16]	64	2.4	1.5	0.9	$V(H) = 0.34$	Prototype	
		2005	Kurchatov Inst. [11]	6	28	11	—	$V(H) = 1.06$	Model	
		2005–07	STFC [19]	20	14	6	—	$V(H) = 0.9$	Model	
		2005–07	STFC [19]	25	12	6	—	$V(H) = 0.53$	Model	
		2005–07	STFC [19]	25	12	6	—	$V(H) = 0.96$	Model	
		2005–07	STFC [19]	42	11.5	6.35	—	$V(H) = 0.82$	Model	
		2008	STFC [19]	150	11.5	6.35	5.23	$V(H) = 1.13$	Prototype	
		2018	ANL [12]	38.5	31.5	31	8	$V(H) = 0.41$	Device	APS
	Nb_3Sn wire	2007	ANL [21]	17	14	7.94	—	$V(H) = 0.9$	Model	
		2012	Ohio State U. [23]	17	14	8	—	$V(H) = 0.8$	Model	
	MgB_2 wire	2009	Ohio State U. [24]	17	14	8	—	$V(H) = 0.25$	Model	
Planar	NbTi wire	1980	PARIS XI [30]	23	40	22	12	$V = 0.45$	Device	
		1990	BNL [51]	3	8.8	4.4	—	$V = 0.5$	Model	
		1996	BNL [52]	23	8.8	4.4	3.8	$V = 0.51$	Prototype	
		1998	KIT [32]	100	3.8	1	1	$V = 0.56$	Device	
		2003	KIT/ACCEL [35]	10	14	5	—	$V = 1.33$	Model	
		2006	KIT/ACCEL [36]	100	14	8	7.4	$V = 0.38$	Device	
		2008	NSRRC [60]	20	15	5.6	—	$V = 1.45$	Model	
		2011	NSRRC [61]	65	15	5.6	—	$V = 1.36$	Model	
		2013	ANL [54]	20.5	16	9.5	7.2	$V = 0.8$	Device	APS
		2015	KIT/Noell [28]	11.5	20	8	—	$V = 1.2$	Model	
		2015	ANL [56]	59.5	18	9.5	7.2	$V = 0.98$	Device	APS
		2016	SINAP [62]	5	16	8	—	$V = 0.93$	Model	
		2016	KIT/Noell [26]	100.5	15	8	7	$V = 0.73$	Device	
		2016	BINP [86]	15	15.6	8	—	$V = 1.2$	Model	
		2018	BINP [87]	40	15.6	8	—	$V = 1.2$	Model	
		2018	ANL [57]	70	21	8	—	$V = 1.67$	Model	
		2019	KIT/Noell [42]	74.5	20	8	7	$V = 1.18$	Device	
		2019	KIT [43]	24 or 12	17 or 34	6	—	$V = 1.3$ or 2.3	Model	
		2019	STFC [48]	19	15.5	7.4	5.4	$V \geqslant 0.8$	Device	
		2021	BINP [88]	119	15.6	8	—	$V = 1.2$	Model	
		2021	SINAP [64]	50	16	10	7.5	$V = 0.62$	Device	
		2021	IHEP [66]	30	15	7	—	$V = 1.01$	Model	
	Nb_3Sn wire	2018	LBNL [48]	73	19	8	—	$V = 1.83$	Model	
		2021	ANL [72]	28.5	18	9.5	—	$V = 1.2$	Model	
	ReBCO tape	2014	LANL [80]	3	14	3.2	—	$V = 0.77$	Model	
		2017	ANL [74]	5	16	9.5	—	$V = > 0.2$	Model	
	ReBCO bulk	2013	Kyoto U. [104]	5	10	4	—	$V = 0.85$	Model	
		2019	PSI [107]	5	10	6	—	$V = 0.85$	Model	
		2021	PSI [3]	10	10	4	—	$V = 1.54$	Model	
Variable	NbTi wire	2010	NSRRC [120]	4.5	24	6.8	—	$V(H) = 0.61$	Model	
		2019	ANL [126]	15	30	—	6	$V(H) = 0.6$	Model	
		2020	BINP [121]	14	22	8	—	$V = 1.0, H = 0.7$	Model	

SCU technology (1/2)

- SCUs in **Synchrotron sources**

- SCU16 developed by SINAP and tested at the Shanghai Synchrotron Radiation Facility (SSRF)
- BINP (Budker Institut of Nuclear Physics) SC wiggler at Diamond Light Source
- KIT Noell:
  - ► SCU installed Australian Light Source
  - ► SC wiggler for NSLSII

K. Zhang and M. Calvi, 2022 Supercond. Sci. Technol. 35 093001

Table 1. Summary of state-of-the-art developed SCU models, prototypes and devices. Model: full SCU coil assembly (testing coils and half coil assemblies are not included). Prototype: full SCU coil assembly + vacuum chamber + cryostat. Device: full SCU coil assembly + vacuum chamber + cryostat + beam commissioned.

SCU type	Conductor	Year	Laboratory	No of periods	Period length (mm)	Magnetic bore/gap (mm)	Vacuum bore/gap (mm)	Peak on-axis field (T)	Type	
Helical	NbTi wire	1973	Stanford U. [9]	160	32.3	9.8	8	$V(H) = 1.30$	Device	
		1974	Stanford U. [9]	160	32.3	12.5	10.2	—	Device	
		1992	BINP [15]	8	24	20	18	$V(H) = 0.47$	Device	
		2002	Cornell U. [16]	64	2.4	1.5	0.9	$V(H) = 0.34$	Prototype	
		2005	Kurchatov Inst. [11]	6	28	11	—	$V(H) = 1.06$	Model	
		2005–07	STFC [19]	20	14	6	—	$V(H) = 0.9$	Model	
		2005–07	STFC [19]	25	12	6	—	$V(H) = 0.53$	Model	
		2005–07	STFC [19]	25	12	6	—	$V(H) = 0.96$	Model	
		2005–07	STFC [19]	42	11.5	6.35	—	$V(H) = 0.82$	Model	
		2008	STFC [19]	150	11.5	6.35	5.23	$V(H) = 1.13$	Prototype	
		2018	ANL [12]	38.5	31.5	31	8	$V(H) = 0.41$	Device	
	Nb_3Sn wire	2007	ANL [21]	17	14	7.94	—	$V(H) = 0.9$	Model	
		2012	Ohio State U. [23]	17	14	8	—	$V(H) = 0.8$	Model	
	MgB_2 wire	2009	Ohio State U. [24]	17	14	8	—	$V(H) = 0.25$	Model	
Planar	NbTi wire	1980	PARIS XI [30]	23	40	22	12	$V = 0.45$	Device	
		1990	BNL [51]	3	8.8	4.4	—	$V = 0.5$	Model	
		1996	BNL [52]	23	8.8	4.4	3.8	$V = 0.51$	Prototype	
		1998	KIT [32]	100	3.8	1	1	$V = 0.56$	Device	
		2003	KIT/ACCEL [35]	10	14	5	—	$V = 1.33$	Model	
		2006	KIT/ACCEL [36]	100	14	8	7.4	$V = 0.38$	Device	
		2008	NSRRC [60]	20	15	5.6	—	$V = 1.45$	Model	
		2011	NSRRC [61]	65	15	5.6	—	$V = 1.36$	Model	
		2013	ANL [54]	20.5	16	9.5	7.2	$V = 0.8$	Device	
		2015	KIT/Noell [28]	11.5	20	8	—	$V = 1.2$	Model	
		2015	ANL [56]	59.5	18	9.5	7.2	$V = 0.98$	Device	
		2016	SINAP [62]	5	16	8	—	$V = 0.93$	Model	
		2016	KIT/Noell [26]	100.5	15	8	7	$V = 0.73$	Device	
		2016	BINP [86]	15	15.6	8	—	$V = 1.2$	Model	
		2018	BINP [87]	40	15.6	8	—	$V = 1.2$	Model	
		2018	ANL [57]	70	21	8	—	$V = 1.67$	Model	
		2019	KIT/Noell [42]	74.5	20	8	7	$V = 1.18$	Device	
		2019	KIT [43]	24 or 12	17 or 34	6	—	$V = 1.3$ or 2.3	Model	
		2019	STFC [48]	19	15.5	7.4	5.4	$V \geqslant 0.8$	Device	
		2021	BINP [88]	119	15.6	8	—	$V = 1.2$	Model	
		2021	SINAP [64]	50	16	10	7.5	$V = 0.62$	Device	SSRF
		2021	IHEP [66]	30	15	7	—	$V = 1.01$	Model	
	Nb_3Sn wire	2018	LBNL [48]	73	19	8	—	$V = 1.83$	Model	
		2021	ANL [72]	28.5	18	9.5	—	$V = 1.2$	Model	
	ReBCO tape	2014	LANL [80]	3	14	3.2	—	$V = 0.77$	Model	
		2017	ANL [74]	5	16	9.5	—	$V = > 0.2$	Model	
	ReBCO bulk	2013	Kyoto U. [104]	5	10	4	—	$V = 0.85$	Model	
		2019	PSI [107]	5	10	6	—	$V = 0.85$	Model	
		2021	PSI [3]	10	10	4	—	$V = 1.54$	Model	
Variable	NbTi wire	2010	NSRRC [120]	4.5	24	6.8	—	$V(H) = 0.61$	Model	
		2019	ANL [126]	15	30	—	6	$V(H) = 0.6$	Model	
		2020	BINP [121]	14	22	8	—	$V = 1.0, H = 0.7$	Model	

SCU technology (2/2)

- SCUs **in FELs**

SCU technology (2/2)

- SCUs **in FELs**
  - IR FEL experiment at Stanford in 1976

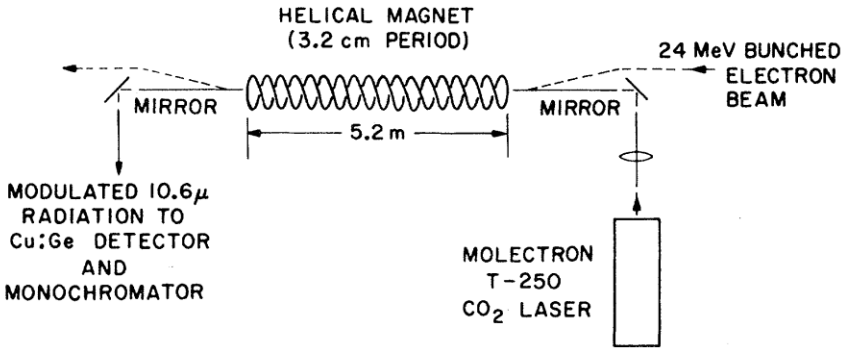

FIG. 1. Experimental setup. The electron beam was magnetically deflected around the optical components on the axis of the helical magnet.

TABLE I. Magnet design parameters.

	Magnet #1	Magnet #2
Helix form material	Aluminum	Delrin
Helix period (cm) at 300°K	3.23	3.23
Number of periods	160	160
Helix form I.D. (cm)	0.98	1.25
Helix form O.D. (cm)	3.20	3.20
Inside radius of first layer (cm)	0.554	0.726
Outside radius of last layer (cm)	1.46	1.39
Helical groove width (cm)	0.60	0.85
Number of layers	9	8
Number of wires per layer	4	8
Wire dimensions (cm × cm)	0.103 × 0.144	0.082 × 0.100
Magnetic field on axis (G/A)	11.1	15.8
I.D. of copper bore (cm)	0.80	1.02

VOLUME 36, NUMBER 13 PHYSICAL REVIEW LETTERS 29 MARCH 1976

Observation of Stimulated Emission of Radiation by Relativistic Electrons in a Spatially Periodic Transverse Magnetic Field*

Luis R. Elias, William M. Fairbank, John M. J. Madey, H. Alan Schwettman, and Todd I. Smith
Department of Physics and High Energy Physics Laboratory, Stanford University, Stanford, California 94305
(Received 15 December 1975)

Gain has been observed for optical radiation at 10.6 μm due to stimulated radiation by a relativistic electron beam in a constant spatially periodic transverse magnetic field. A gain of 7% per pass was obtained at an electron current of 70 mA. The experiments indicate the possibility of a new class of tunable high-power free-electron lasers.

Superconducting helically wound magnet for the free-electron laser

L. R. Elias and J. M. Madey
High Energy Physics Laboratory, Stanford University, Stanford, California 94305
(Received 12 April 1979; accepted for publication 18 May 1979)

Theoretical and experimental studies conducted by the Stanford Free Electron Laser group have resulted in the first operation of a free-electron laser amplifier and free-electron laser oscillator. Two superconducting helically wound periodic magnetics have been constructed for use with the laser. In this paper we present a discussion of design considerations and test results for the two magnets. The tests included measurement of the magnitude and the variation of the transverse magnetic field with radius in the bore of the magnets, the critical current, and the intensity, angular distribution, and spectrum of the spontaneous radiation emitted by electrons moving through the field.

SCU technology (2/2)

- SCUs **in FELs**:
  - IR FEL experiment at Stanford in 1976

VOLUME 36, NUMBER 13 PHYSICAL REVIEW LETTERS 29 MARCH 1976

Observation of Stimulated Emission of Radiation by Relativistic Electrons in a Spatially Periodic Transverse Magnetic Field*

Luis R. Elias, William M. Fairbank, John M. J. Madey, H. Alan Schwettman, and Todd I. Smith
Department of Physics and High Energy Physics Laboratory, Stanford University, Stanford, California 94305
(Received 15 December 1975)

Gain has been observed for optical radiation at 10.6 μm due to stimulated radiation by a relativistic electron beam in a constant spatially periodic transverse magnetic field. A gain of 7% per pass was obtained at an electron current of 70 mA. The experiments indicate the possibility of a new class of tunable high-power free-electron lasers.

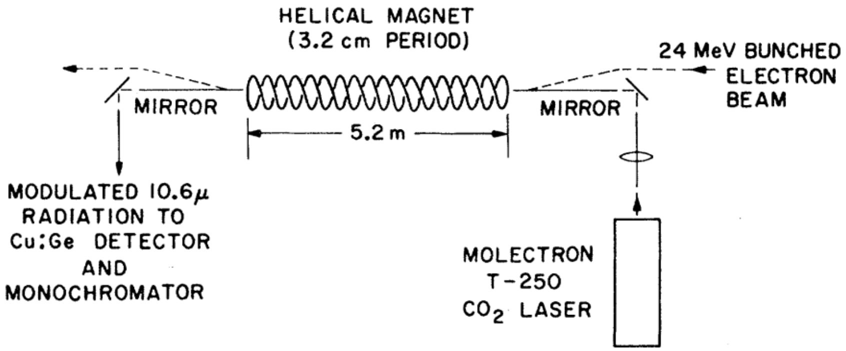

FIG. 1. Experimental setup. The electron beam was magnetically deflected around the optical components on the axis of the helical magnet.

TABLE I. Magnet design parameters.

	Magnet #1	Magnet #2
Helix form material	Aluminum	Delrin
Helix period (cm) at 300°K	3.23	3.23
Number of periods	160	160
Helix form I.D. (cm)	0.98	1.25
Helix form O.D. (cm)	3.20	3.20
Inside radius of first layer (cm)	0.554	0.726
Outside radius of last layer (cm)	1.46	1.39
Helical groove width (cm)	0.60	0.85
Number of layers	9	8
Number of wires per layer	4	8
Wire dimensions (cm × cm)	0.103 × 0.144	0.082 × 0.100
Magnetic field on axis (G/A)	11.1	15.8
I.D. of copper bore (cm)	0.80	1.02

Superconducting helically wound magnet for the free-electron laser

L. R. Elias and J. M. Madey
High Energy Physics Laboratory, Stanford University, Stanford, California 94305
(Received 12 April 1979; accepted for publication 18 May 1979)

Theoretical and experimental studies conducted by the Stanford Free Electron Laser group have resulted in the first operation of a free-electron laser amplifier and free-electron laser oscillator. Two superconducting helically wound periodic magnetics have been constructed for use with the laser. In this paper we present a discussion of design considerations and test results for the two magnets. The tests included measurement of the magnitude and the variation of the transverse magnetic field with radius in the bore of the magnets, the critical current, and the intensity, angular distribution, and spectrum of the spontaneous radiation emitted by electrons moving through the field.

  - STFC at Daresbury : SCU test at CLARA linac
  - Prototype for LCLS (collaboration ANL, LBNL and SLAC) + LCLS facility plans to install a cryostat with two 1.5m long SCU coils and cold intersection
  - Prototype HTSC-bulk SCU for SwissFEL to be tested first at Swiss Light Source
  - SHINE (Shanghai HIgh repetition rate XFEL aNdExtreme light facility): 40 in-vacuum SCUs, 16mm period, B=0.682 – 1.583 T, photon energy = 10-25keV, magnetic length: 4m (phase shifter in the middle)

SCUs as part of the European XFEL facility development program

- European XFEL has the highest beam energy among XFELs:
  - **Opportunity** to produce **photons** with energies in the range **30-100 keV**
    - ► MHz rate X-ray microscopy can reveal bulk dynamics in material such as crack propagation or shockwave propagation previously possible to observe only ex-situ

- European XFEL has two hard and one soft X-ray beamlines:
  - The state of the art SCU technology offers a solution to cover the present **range of photons in all beamlines** with **fixed e-beam energy of 8.5 GeV**.

- CW upgrade of the linac at 7-8 GeV is presently under consideration:
  - SCU SASE line NbTi at 2 K with 15 mm period and 5 mm vacuum gap can potentially cover from 8.6 keV up to 25 keV, a similar range as with the existing SASE1/2 lines with permanent magnet undulators with 40 mm period length.

Numerical studies: a hard X-ray SCU SASE line for the future

- Generation of hard X rays up to ~ 100 keV for strategic upgrade plans
  - **NbTi** at **2K** SCUs with a period length of **15 mm** and a vacuum gap of 5 mm allow covering a range between **54 keV and 100 keV**.
  - Numerical studies show that hard X-rays generation could be possible with “almost” state-of-the-art technology.

39th Free Electron Laser Conf. FEL2019, Hamburg, Germany JACoW Publishing
ISBN: 978-3-95450-210-3 doi:10.18429/JACoW-FEL2019-TUP061

SUPER-X: SIMULATIONS FOR EXTREMELY HARD X-RAY GENERATION WITH SHORT PERIOD SUPERCONDUCTING UNDULATORS FOR THE EUROPEAN XFEL

S. Serkez*, G. Geloni, S. Karabekyan, Y. Li, T. Tanikawa,
S. Tomin, F. Wolff-Fabris, European XFEL, Schenefeld, Germany
S. Casalbuoni, KIT, Karlsruhe, Germany
C. Boffo†, Bilfinger Noell, Würzburg, Germany
M. Dohlus, E. Schneidmiller, M. Yurkov, I. Zagorodnov, DESY, Hamburg, Germany
A. Trebushinin, BINP, Novosibirsk, Russia

14th International Conference on Synchrotron Radiation Instrumentation (SRI 2021) IOP Publishing
Journal of Physics: Conference Series **2380** (2022) 012011 doi:10.1088/1742-6596/2380/1/012011

Analysis of the error budget for a superconducting undulator SASE line at European XFEL

B. Marchetti, S. Casalbuoni, V. Grattoni, S. Serkez
European XFEL GmbH, 22869 Schenefeld, Germany

A pre-series prototype for the superconducting undulator afterburner for the European XFEL

S. Casalbuoni[1], J. Baader[1], G. Geloni[1], V. Grattoni[1], W. Decking[2], D. La Civita[1], C. Lechner[1], L. Lilje[2], S. Liu[2], B. Marchetti[1], A. Potter[3], E. Schneidmiller[2], S. Serkez[1], H. Sinn[1], T. Wohlenberg[2] and I. Zagorodnov[2]

[1]European XFEL GmbH, Holzkoppel 4, 22869 Schenefeld, Germany
[2]DESY, Notkestraße 85, 22607 Hamburg, Germany
[3]University of Liverpool, Liverpool L69 3BX, United Kingdom

Pilot project: FESTA Afterburner for SASE2

- **FESTA (Free Electron laser SuperconducTing undulator Afterburner)**
  - Installation of **1+5 cryomodules (i.e. 2+10 undulator)** at SASE2 for photon energies higher than 40 keV.
  - Demonstration of the operation of SCUs in X-rays FELs.
  - Cover the complete photon energy range of soft X-ray experiments without changing the beam energy.

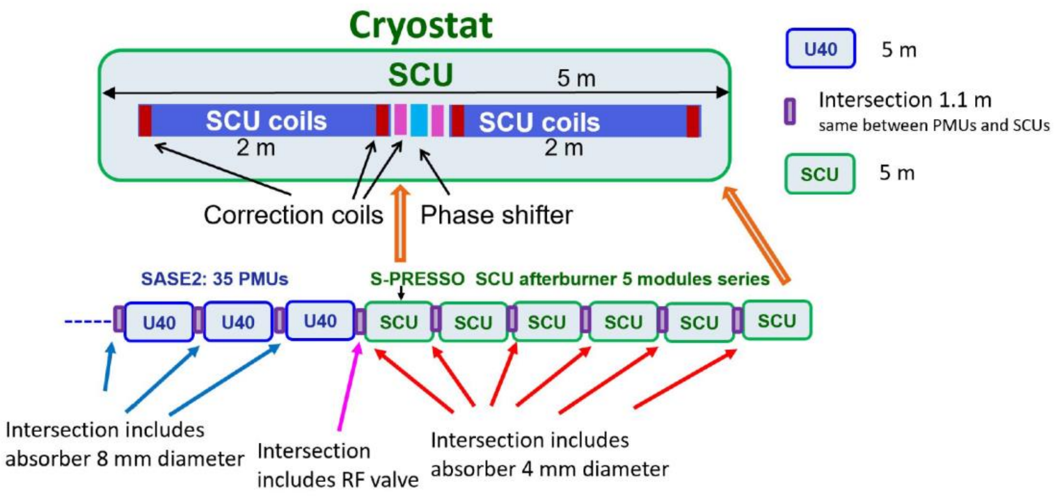

S-PRESSO (Superconducting undulator PRE-SerieS mOdule) is the prototype module, already in production (contract assigned to Bilfinger Noell GmbH).
S-PRESSO will include **NbTi coils** and work at **4K**.

Table 2. Main Parameters of S-PRESSO

Period	18 mm
Peak field	1.82 T
K	3.06
Vacuum gap	5 mm
First field int. (x,y)	$< 4 \times 10^{-6}$ T m
Second field int. (x,y)	$< 10^{-4}$ T m^2
$\Delta K/K$ rms	< 0.0015
Roll off at ± 2 mm	$< 5 \times 10^{-5}$
Beam heat load	10 W

A pre-series prototype for the superconducting undulator afterburner for the European XFEL

S. Casalbuoni[1], J. Baader[1], G. Geloni[1], V. Grattoni[1], W. Decking[2], D. La Civita[1], C. Lechner[1], L. Lilje[2], S. Liu[2], B. Marchetti[1], A. Potter[3], E. Schneidmiller[2], S. Serkez[1], H. Sinn[1], T. Wohlenberg[2] and I. Zagorodnov[2]

[1]European XFEL GmbH, Holzkoppel 4, 22869 Schenefeld, Germany
[2]DESY, Notkestraße 85, 22607 Hamburg, Germany
[3]University of Liverpool, Liverpool L69 3BX, United Kingdom

Pilot project: FESTA Afterburner for SASE2

- FESTA (Free Electron laser SuperconducTing undulator Afterburner)

Expected performances obtained from numerical simulations in terms of number pf photons per radiation pulse.

Energy	16.5 GeV
Normalized emittance	0.4 mm mrad
Initial energy spread	3 MeV
Current	5 kA
Bunch length	30 fs

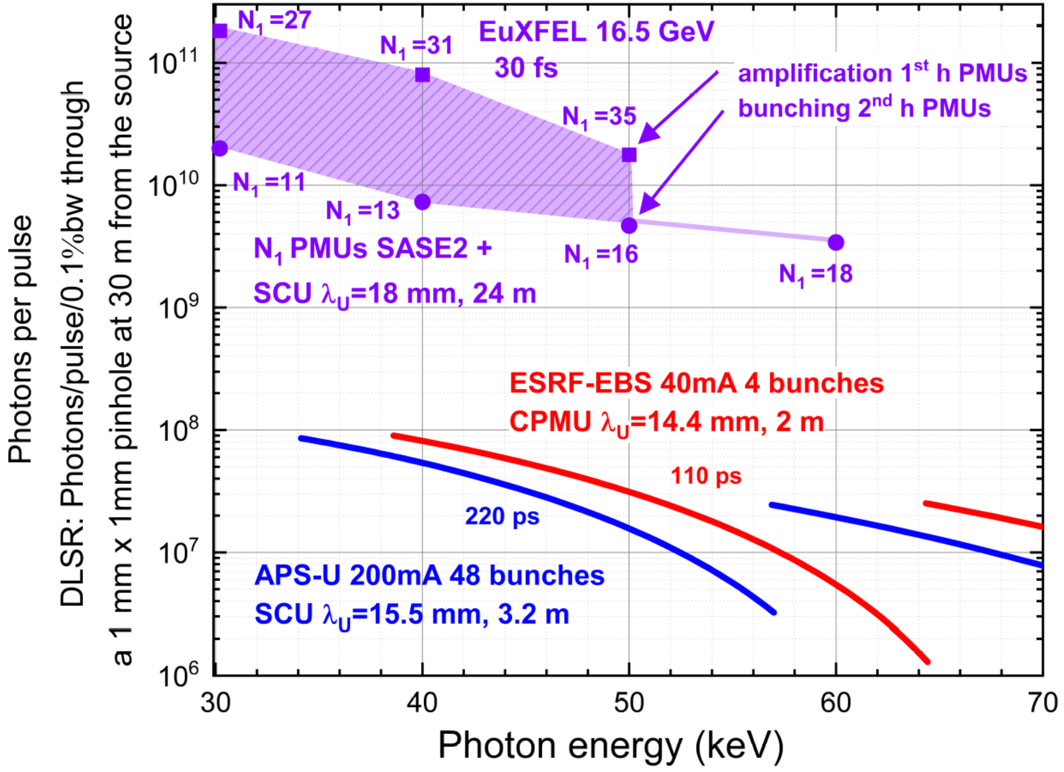

Numerical simulations by C. Lechner.

More Technical Details on the Studies done on Magnet Tolerances

14th International Conference on Synchrotron Radiation Instrumentation (SRI 2021) IOP Publishing
Journal of Physics: Conference Series **2380** (2022) 012009 doi:10.1088/1742-6596/2380/1/012009

Simulation studies of superconducting afterburner operation for the European XFEL

C Lechner, S Casalbuoni, G Geloni, B Marchetti, S Serkez and H Sinn
European XFEL, Holzkoppel 4, 22869 Schenefeld, Germany

14th International Conference on Synchrotron Radiation Instrumentation (SRI 2021) IOP Publishing
Journal of Physics: Conference Series **2380** (2022) 012010 doi:10.1088/1742-6596/2380/1/012010

An analytical study to determine the mechanical tolerances for the afterburner superconducting undulators at EuXFEL

V. Grattoni, S. Casalbuoni, B. Marchetti
European XFEL GmbH, Holzkoppel 4, 22869, Schenefeld

13th Int. Particle Acc. Conf. IPAC2022, Bangkok, Thailand JACoW Publishing
ISBN: 978-3-95450-227-1 ISSN: 2673-5490 doi:10.18429/JACoW-IPAC2022-THPOPT060

TOLERANCE STUDY ON THE GEOMETRICAL ERRORS FOR A PLANAR SUPERCONDUCTING UNDULATOR

V. Grattoni*, S. Casalbuoni, B. Marchetti, European XFEL, Schenefeld, Germany

V. Grattoni et al. „Effect of SCU long range errors on the FEL performance“
In proceedings IPAC23.

Effect of Magnetic Field Errors in FEL Process – Qualitative View

Random errors ΔK(z)

Effect in „transverse e-beam motion“

- **“Random walk”** component in the **electron orbit**
- **Non-zero first and second field integrals** at the exit of the undulator (**$I_{1x}(z_f)$, $I_{1y}(z_f)$, $I_{2x}(z_f)$, $I_{2y}(z_f)$**)
- The electron beam exits the undulator with a **parasitic transverse angle** and a **parasitic transverse offset**

- We can make

  $I_{1x}(z_f) = I_{1y}(z_f) = I_{2x}(z_f) = I_{2y}(z_f) = 0$

  by adjusting entrance/exit coils of the undulator;

- The electron beam exits the undulator with **zero angle and zero offset**.

The central excursion in trajectory affects the overlap between beam and radiation !

Effect in „time“

Random error in the **transverse velocity** of the electrons in the undulator: **$\Delta\beta_x(z)$**

Random error in the **time-of-flight** of the electrons in the undulator: **t(z)**

phase noise in the emission process

Reduction of the peak power radiated

Definition first and second magnetic field integrals:

$$I_{1x}(z) = \int_0^z B_x(z_1)dz_1$$

$$I_{1y}(z) = \int_0^z B_y(z_1)dz_1$$

$$I_{2x}(z) = \int_0^z \int_0^{z_2} B_x(z_1)\,dz_1dz_2$$

$$I_{2y}(z) = \int_0^z \int_0^{z_2} B_y(z_1)\,dz_1dz_2$$

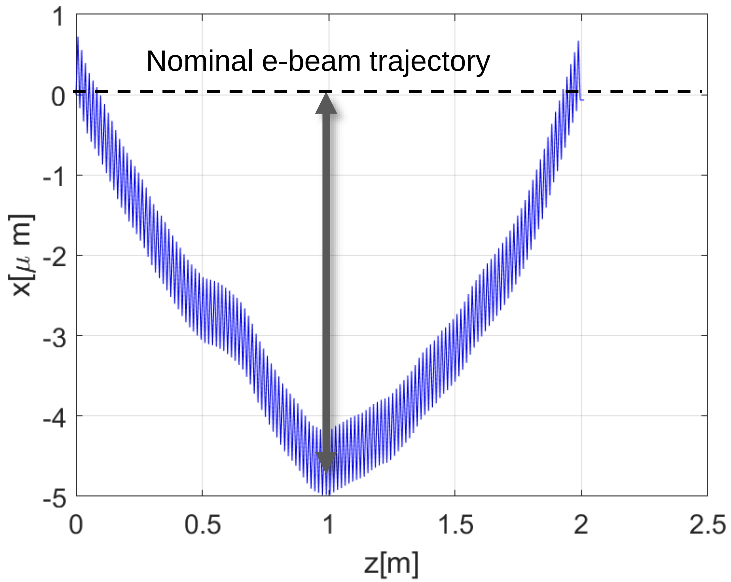

Characterization of the magnetic fields: a key step to understand and evaluate the SCU technology

- Numerical simulations hint us that **precision in the manufacture** of the coils and their relative **alignment** as well as the alignment with the electron beam and radiation seed pulse are **key to success** for the production of **hard X-rays in FELs**.
- **Early/fast characterization** of the **„stand alone“ coil** (before installation in the final cryostat) allows prompt evaluation of the magnet properties.
  - Magnetic correction procedures (**shimming**) or **discard of the coil** could possibly be applied.
- Characterization of the **final undulator cryostat** including all coils (**main SCU coils, correction coils, phase shifter**) allows to **check the alignment** of the coils and to **calibrate the settings of the currents** to avoid non-zero field integrals in beam axis.

SUNDAE: Superconducting UNDulAtor Experiment

Two test-stands for the precise characterization of the magnetic field of superconducting coils.

SUNDAE1/2 will be installed in the Hall 3 in Bld. 28 at DESY

SUNDAE1:
- Coil in Superfluid Liquid Helium bath
- Single magnet training/characterization
- Magnetic field characterization using Hall-probe measurement

SUNDAE2:
- Coils conduction-cooled via cryocoolers or cryogenic plant (upgrade)
- Characterization of all magnets in the final cryostat
- Magnetic field measurement with Hall-probe, Pulsed-Wire and Moving-Wire Methods.

14th International Conference on Synchrotron Radiation Instrumentation (SRI 2021) IOP Publishing
Journal of Physics: Conference Series 2380 (2022) 012027 doi:10.1088/1742-6596/2380/1/012027

Conceptual Design of a Liquid Helium Vertical Test-Stand for 2m long Superconducting Undulator Coils

B. Marchetti[1], S. Abeghyan[1], J. Baader[1], S. Barbanotti[2], S. Casalbuoni[1], M. Di Felice[1], H.-J. Eckoldt[2], U. Englisch[1], V. Grattoni[1], A. Grau[3], A. Hauberg[2], K. Jensch[2], D. La Civita[1], S. Lederer[2], L. Lilje[2], R. Ramalingam[2], T. Schnautz[2], M. Vannoni[1], M. Yakopov[1], R. Zimmermann[2], P. Ziolkowski[1]
[1] European XFEL GmbH, 22869 Schenefeld, Germany
[2] Deutsches Elektronen-Synchrotron, 22607 Hamburg, Germany
[3] Karlsruher Institut fuer Technologie, D-76021 Karlsruhe, Germany

13th Int. Particle Acc. Conf. IPAC2022, Bangkok, Thailand JACoW Publishing
ISBN: 978-3-95450-227-1 ISSN: 2673-5490 doi:10.18429/JACoW-IPAC2022-THPOPT032

SUNDAE2 AT EuXFEL: A TEST STAND TO CHARACTERIZE THE MAGNETIC FIELD OF SUPERCONDUCTING UNDULATORS

J. E. Baader*, S. Abeghyan, S. Casalbuoni, D. La Civita, B. Marchetti, M. Yakopov, P. Ziolkowski, European XFEL GmbH, Schenefeld, Germany
H.-J. Eckoldt, A. Hauberg, S. Lederer, L. Lilje, T. Wohlenberg, R. Zimmermann, DESY, Hamburg, Germany
A. W. Grau, Karlsruhe Institute of Technology, Karlsruhe, Germany

SUNDAE1: Overview

- Coil in **Liquid Helium bath**
  - → **Superfluid He bath (2K)**
- **Linear motion system (LMS)** holding two **Hall probes** for magnet characterization.

Minimum magnetic gap: 6mm

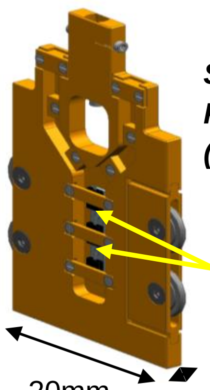

Sledge design Final version (P. Ziolkowski)

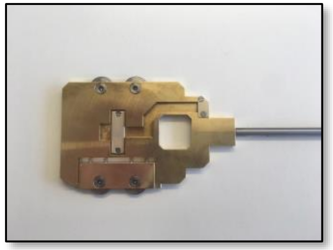

Sledge - Production test

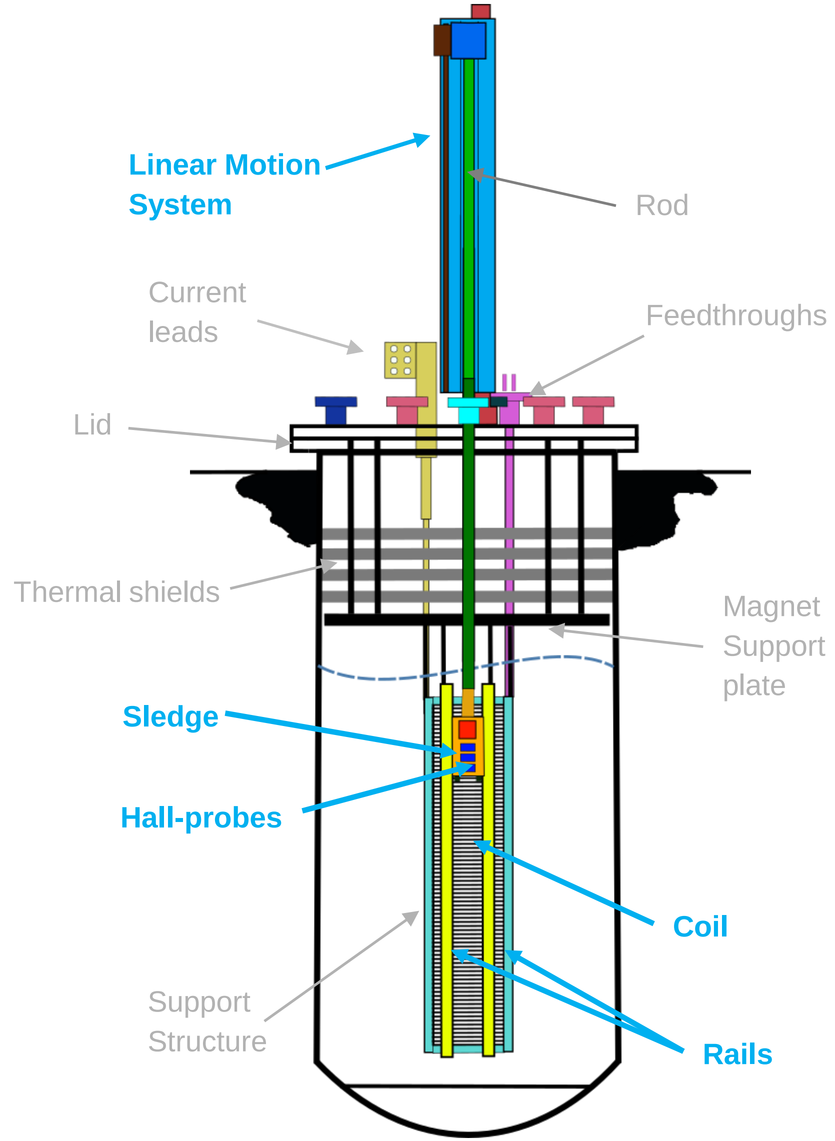

*Characterization of the vertical component of the magnetic field with **Hall-probe measurement**:*

Range of the longitudinal scan	2.3m
Resolution of the magnetic field*	0.1mT
Goal resolution of the position of the probe	1 µm

*limited by Hall probe calibration error

For S-PRESSO:

- B=1.82T → Requested field quality $\Delta B/B << 10^{-3}$ → $B_{res} << 1.8mT$
- λ_{und} = 18mm → Res. Hall-probe position << 1/10 * λ_{und} /2 = 0.9 mm
- Accuracy Hall-probe position << Tolerance on pole/groove width = 10µm

SUNDAE2 – Conceptual view

Figure courtesy J. Baader

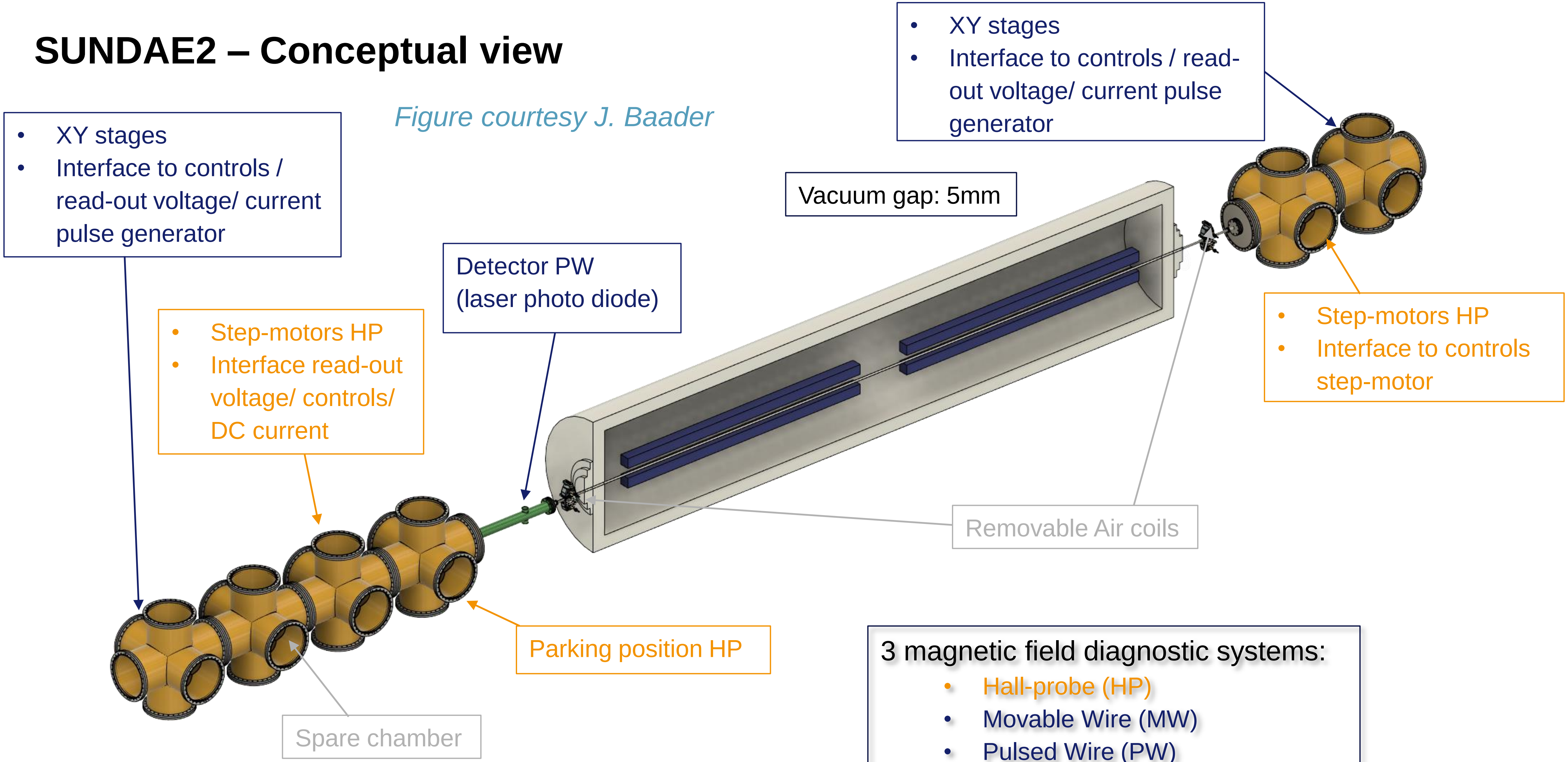

3 magnetic field diagnostic systems:

- Hall-probe (HP)
- Movable Wire (MW)
- Pulsed Wire (PW)

Overview of Measurements of the Magnetic Field at SUNDAE2

Figure Reference: A. Jain USPAS 2003

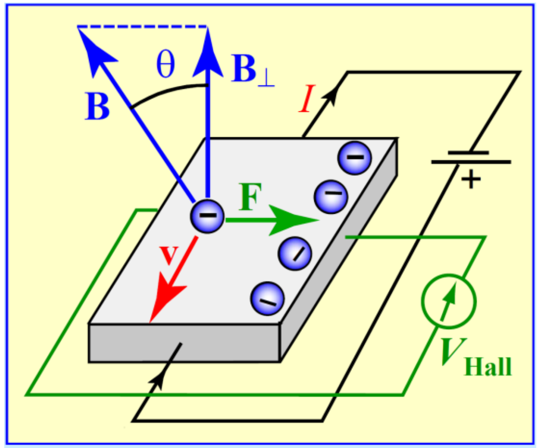

Hall probe

Figure Reference: D. Zangrando, R. P. Walker NIM A 376 (1996)

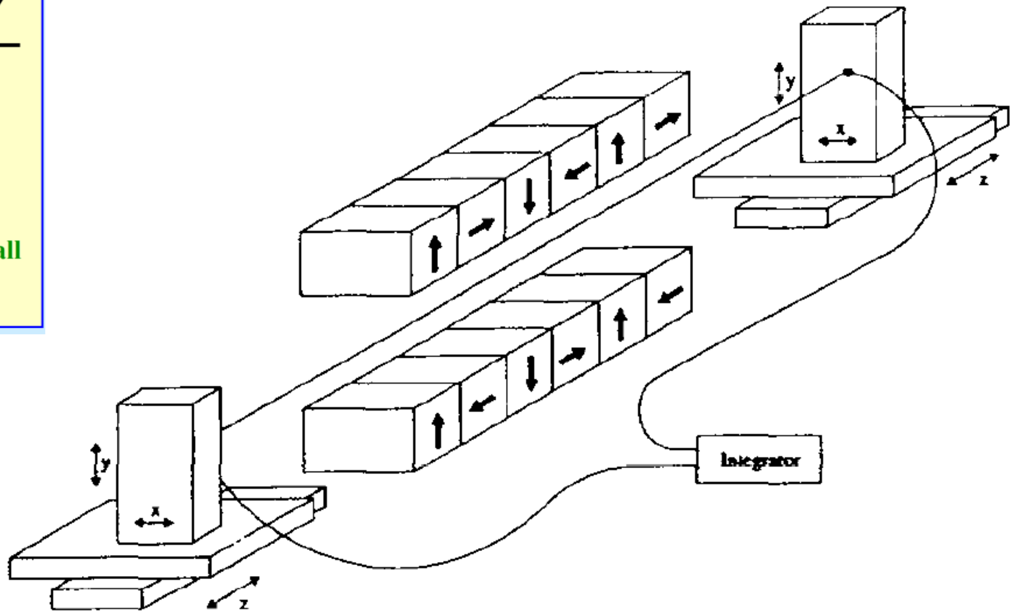

Fig. 1. Schematic showing the measurement of an insertion device with the stretched wire system.

Movable Wire

Figure Reference: J. Baader, S. Casalbuoni, WEPAB126, IPAC21

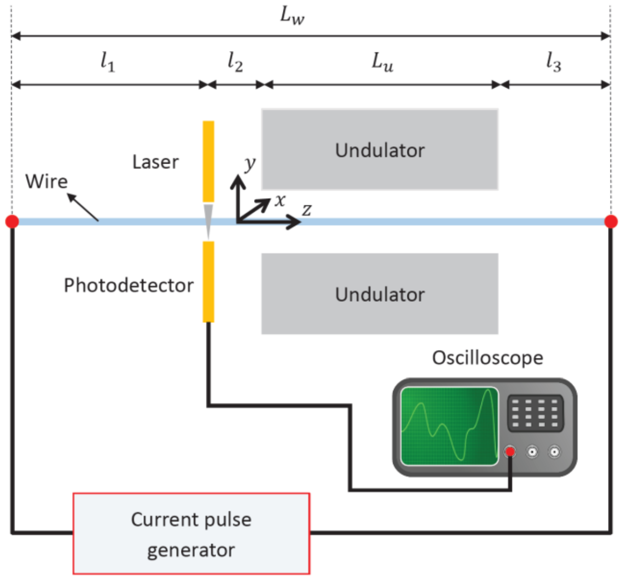

Figure 1: Two-dimensional scheme of the pulsed wire system and main lengths.

Pulsed Wire

Overview of Measurements of the Magnetic Field at SUNDAE2

Technique	How it is used
Hall Probe	• Local Field Amplitude in the vertical plane • Accuracy field measurement ~ 0.1 mT (calibration error) • Precision Hall probe position ~ 1 µm
Movable Wire	• Measurement of first and second magnetic field integrals in both transverse planes • Best accuracy for measuring field integrals. • Goal resolution: I_{1x}, I_{1y}=4*10^{-6}Tm, I_{2x}, I_{2y}=1*10^{-4}Tm^2 • Used for finding optimal values of correction coils and phase shifter current
Pulsed Wire	• Space resolved field integrals on both transverse planes as well as magnetic field profile can be measured • Development for the characterization of small aperture magnets (LEAPS-INFRAINNOV) • Faster than Hall probe

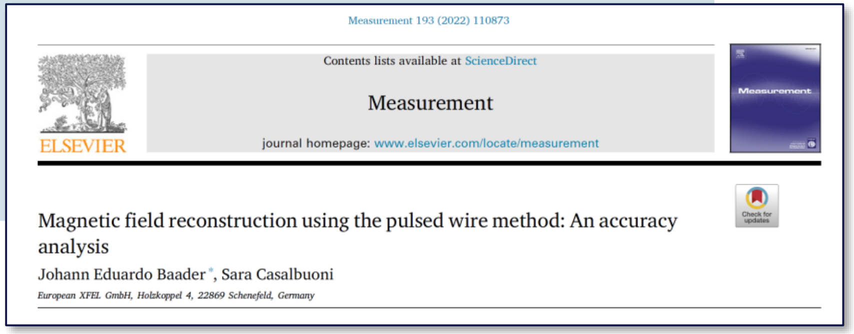

Measurement 193 (2022) 110873

Contents lists available at ScienceDirect

ELSEVIER

Measurement

journal homepage: www.elsevier.com/locate/measurement

Magnetic field reconstruction using the pulsed wire method: An accuracy analysis

Johann Eduardo Baader *, Sara Casalbuoni

European XFEL GmbH, Holzkoppel 4, 22869 Schenefeld, Germany

Summary and Conclusions

- European XFEL is developing **SCU technology** for the future upgrade of its beamlines:
  - SCU can potentially allow to fully exploit the high energy of the electron-beam for production **of very hard X-rays (towards 100 keV photon energy)**
  - SCU would allow to shift the tuning-mechanism from the electron beam side (electron energy) to the undulators side (magnetic field), thus **reducing the complexity of the machine setup** for the different photon beamlines.
- As **pilot project** an **SCU afterburner for SASE2 (FESTA)** at European has been proposed and studied. The **prototype cryomodule S-PRESSO** is already under production by Bilfinger Noell GmbH.
- Two **test-stands** for the characterization of the SCU coils (**SUNDAE1 and SUNDAE2**) are been realized on the **DESY campus**. The installation of the major components of SUNDAE1 expected in 2023, while the major components of SUNDAE2 are expected to be installed in 2024.

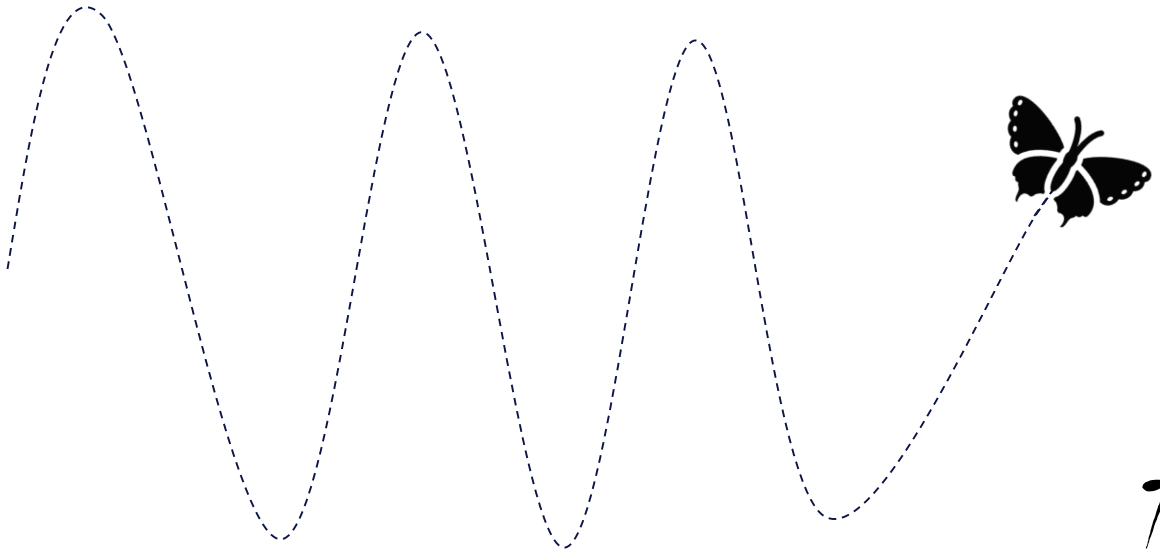

Thank you for your attention!